A study of the polarized structure function $g_1^{\mathrm{p}}(x, Q^2)$ and the polarized gluon distribution $\Delta g(x, Q^2)$ at HERA

A. De Roeck[1,2], A. Deshpande[3], V.W. Hughes[3], J. Lichtenstadt[4], G. Rädel[2]

[1] Deutsches Elektronen-Synchroton DESY, Notkestr. 85, 22603 Hamburg, Germany
[2] CERN, Div. PPE, 1211 Genève 23, Switzerland
[3] Department of Physics, Yale University, New Haven, CT 06520, USA
[4] School of Physics and Astronomy, The Raymond and Beverly Sackler Faculty of Exact Sciences, Tel Aviv University, Tel Aviv 69978, Israel

Abstract. We present estimates of possible data on spin-dependent asymmetries in inclusive scattering of high energy polarized electrons by high energy polarized protons at HERA with their statistical errors and discuss systematic errors. We show that these data will provide important information on the low-x behavior of the polarized structure function g_1, and will reduce the uncertainty in the determination of the first moment of the polarized gluon distribution $\Delta g(x, Q^2)$ obtained from the QCD analysis of g_1 in NLO. Furthermore, using asymmetries for di-jet events from a polarized HERA would substantially reduce the uncertainty in the shape of $\Delta g(x, Q^2)$. Use of the information on $\Delta g(x, Q^2)$ from the di-jet analysis in conjunction with the NLO QCD analysis of g_1 will provide an accurate determination of $\Delta g(x, Q^2)$ and its first moment.

1 Introduction

Measurements of nucleon structure functions by lepton-nucleon inclusive electromagnetic deep inelastic scattering (DIS) were of fundamental importance in studying nucleon structure and have provided crucial information for the development of perturbative QCD (pQCD). The history of these experiments over the past 40 years has shown that important new information has been obtained when measurements were extended to new kinematic regions. In the mid-1950's at Stanford, measurements of elastic electron-proton scattering were extended to a higher Q^2 range of 1 $(\mathrm{GeV/c})^2$ and for the first time it was observed that the proton has a finite size [1]. In the late 1960's at SLAC the extension of measurements of inelastic inclusive electron scattering to the deep inelastic region of $Q^2 > 1$ $(\mathrm{GeV/c})^2$ led to the discovery of the parton substructure of the proton [2]. This substructure was further studied in muon-nucleon deep inelastic scattering [3]. The extension of the data to lower x and higher Q^2 made possible by the HERA ep-collider showed a surprisingly steep rise towards low x of the unpolarized structure function F_2 [4] whose explanation has led to an improved understanding of perturbative QCD. Furthermore, these data as well as data from di-jet production [5] enabled a precise determination of the gluon density in the nucleon.

Polarized DIS, which measures the spin dependent structure function of the nucleon has a similar history. The first measurements by the Yale-SLAC collaboration

[6] extended down to $x = 0.1$ and were consistent with the naive quark-parton model view that the nucleon spin is carried by its constituent quarks. These experiments were followed up at CERN by the EM Collaboration [7] extending the measurements to lower x of 0.01. The results showed that the Ellis-Jaffe sum rule is violated, which within the quark parton model implied that the contribution of the quark spins $\Delta\Sigma$ to the proton spin is small. This surprising result stimulated a large amount of experimental and theoretical work on polarized structure functions [8]. The next generation of experiments by the SM Collaboration at CERN [9,10], by the SLAC collaborations [12,11,13], and by the HERMES collaboration at DESY [14] reduced significantly the statistical and systematic uncertainties on the measurements and the kinematic range was extended to $x = 0.003$. In addition, spin structure functions for the deuteron and neutron as well as the proton were measured, thereby providing the first experimental verification of the fundamental model-independent Bjorken sum-rule. On the theory side, in the QCD quark parton model, the breaking of the Ellis-Jaffe sum rule can be interpreted as due to a positively polarized gluon distribution and/or a negatively polarized strange quark contribution. Hence precise information on the polarized gluon distribution is important for the understanding of the spin structure of hadrons, and will be studied in this paper.

Despite the recent experimental progress, the polarized structure functions are still measured in a limited x and Q^2 range and a large uncertainty on the first moment

of g_1 comes from the unknown low-x behavior of g_1. The kinematic range accessible by present-day fixed target experiments is limited and therefore to obtain a significant extension of the kinematic range the scattering of polarized electrons by polarized protons must be studied in a collider mode such as HERA. While the polarized quark distributions Δq are accessible in fixed target experiments from measurements of g_1, the polarized gluon distribution Δg is deduced from scaling violations of g_1. However, the good quality data on g_1 in the present kinematic range allows us to perform complete next-to-leading order (NLO) QCD analyses of the Q^2 dependence of g_1. Recently several such analyses have been performed [15–18] and have provided the first information on the first moment of the polarized gluon distribution, $\int_0^1 \Delta g(x)\mathrm{d}x$. These analyses suggest a fairly large contribution of the gluon to the spin of the proton [10,19]. Nevertheless the uncertainties are very large and the shape of $\Delta g(x)$ is poorly constrained. This analysis would benefit greatly from additional data over a wider kinematic range.

The HERA collider at DESY provides 27.5 GeV electrons and 820 GeV protons. At present the proton beam at HERA is unpolarized whereas the electron/positron beam has a natural transverse polarization, which can be rotated into a longitudinal polarization in the interaction regions. Once the protons in the HERA ring are polarized it will be possible to measure polarization asymmetries and thus explore spin dependent structure functions in the full HERA kinematic range. The possible extension in the measured $x - Q^2$ range for spin structure function measurements is shown in Fig. 1. The scientific and technical problems involved in obtaining polarized protons in the HERA ring have been discussed in [20]. The measurability of the polarized structure functions at HERA has first been discussed in [21–23].

In this paper we study the potential impact of a polarized HERA on the knowledge of the polarized structure function and the polarized gluon distribution in the proton. We first show that g_1 data from polarized colliding beam experiments at HERA would provide information on the low-x behavior of g_1 and through QCD analyses of g_1 would substantially improve the determination of the first moment of the polarized gluon distribution. We present for the first time an analysis which includes $\Delta g(x, Q^2)$ measurements from di-jet asymmetries together with the QCD analysis of g_1 data from fixed target experiments and from HERA. The determination of the polarized gluon distribution $\Delta g(x, Q^2)$ and its first moment improves substantially when using such a combined analysis.

2 Current status of polarized parton distributions

The structure function g_1 is related to the polarized quark and gluon distributions through

$$g_1(x, t) = \tfrac{1}{2}\langle e^2 \rangle \int_x^1 \frac{\mathrm{d}y}{y}\Big[C_q^{\mathrm{S}}(\tfrac{x}{y}, \alpha_s(t))\Delta\Sigma(y, t)$$
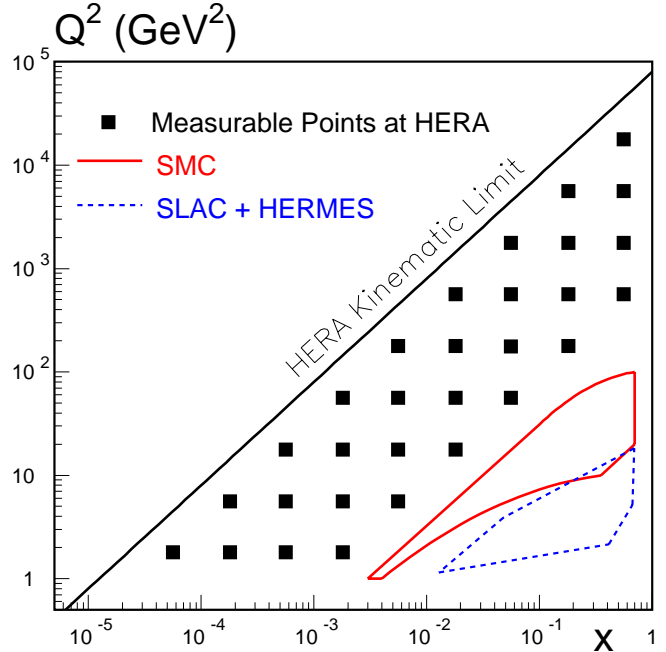

Fig. 1. Measurable $x - Q^2$ region with polarized HERA shown with the presently explored regions by CERN(SMC), SLAC and DESY(HERMES) experiments, and the kinematic limit of measurability at HERA

$$+ 2n_f C_g(\tfrac{x}{y}, \alpha_s(t))\Delta g(y, t)$$
$$+ C_q^{\mathrm{NS}}(\tfrac{x}{y}, \alpha_s(t))\Delta q^{\mathrm{NS}}(y, t)\Big], \qquad (1)$$

where $\langle e^2 \rangle = n_f^{-1}\sum_{k=1}^{n_f} e_k^2$, $t = \ln(Q^2/\Lambda^2)$, $\Delta\Sigma$ and Δq^{NS} are the singlet and non-singlet polarized quark distributions:

$$\Delta\Sigma(x, t) = \sum_{i=1}^{n_f} \Delta q_i(x, t),$$

$$\Delta q^{\mathrm{NS}}(x, t) = \sum_{i=1}^{n_f} (e_i^2/\langle e^2 \rangle - 1)\Delta q_i(x, t),$$

and $C_q^{\mathrm{S,NS}}(\alpha_s(Q^2))$ and $C_g(\alpha_s(Q^2))$ are the quark and gluon coefficient functions.

The x and Q^2 evolution of the polarized quark and gluon distributions is given by the DGLAP evolution equations [24]. The full set of coefficient functions [25] and splitting functions [26] has been computed up to next-to-leading order in α_s. At NLO splitting functions, coefficient functions and parton distributions depend on the renormalization and factorization scheme. The scheme choice is arbitrary and parton distributions in different factorization schemes are related to each other by well-defined linear transformations.

The polarized parton distributions can be obtained by fitting the experimental spin structure function data. The distributions are parametrized at an initial scale and are evolved using the DGLAP equations to values of x and Q^2 of the data, varying the parameters to fit the experimental values of g_1 [15–17]. Here we follow the procedure used

Table 1. Results from the NLO QCD fit to all available published data compared to the results from a fit including also projected data from HERA. The parameters $\eta_{NS}^{p;n}$ are fixed by the octet hyperon β decay constants: $g_A = F + D = 1.2601 \pm 0.0025$ [29] and $F/D = 0.575 \pm 0.016$ [30], $(a_8 = 3F - D)$. The parameter η_g is the first moment of the gluon distribution. All values of the parameters are given at $Q^2 = 1$ GeV^2. Errors reflect the statistical and systematic errors on the data

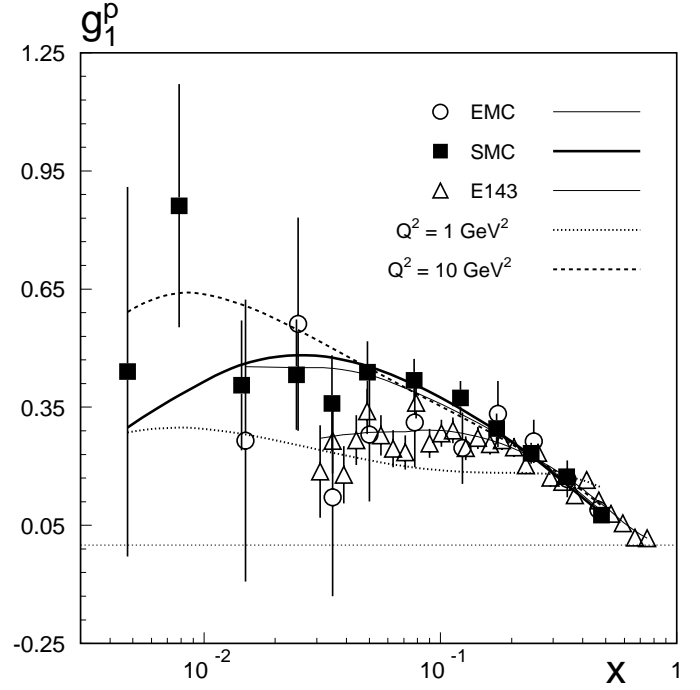| Parameter	Fit to [7,9,10,12,11,13,14]			HERA $\mathcal{L} = 500$ pb^{-1}		
η_g	0.9	$\pm$	0.3	0.9	$\pm$	0.2
η_q	0.40	$\pm$	0.04	0.38	$\pm$	0.03
$\eta_{NS}^{p(n)}$		$+(-)\frac{3}{4}g_A + \frac{1}{4}a_8$			$+(-)\frac{3}{4}g_A + \frac{1}{4}a_8$	
α_g	-0.5	$\pm$	0.3	-0.6	$\pm$	0.1
α_q	0.7	$\pm$	0.3	0.9	$\pm$	0.3
α_{NS}^p	-0.1	$\pm$	0.1	-0.1	$\pm$	0.1
α_{NS}^n	-0.1	$\pm$	0.2	0.1	$\pm$	0.2
β_g		4.0 (fixed)			4.0 (fixed)	
β_q	1.3	$\pm$	0.7	1.5	$\pm$	0.7
β_{NS}^p	1.5	$\pm$	0.3	1.4	$\pm$	0.3
β_{NS}^n	2.6	$\pm$	0.6	2.6	$\pm$	0.6
a_q	-1.4	$\pm$	0.1	-1.4	$\pm$	0.1

Fig. 2. The NLO fit to proton g_1^p data. The solid lines are the fit to the data at measured Q^2 values, and the dashed and the dotted lines are the fit evolved to $Q^2 = 1$ and 10 GeV^2 respectively

in [15]. The initial parametrization at $Q^2 = 1$ GeV^2 is assumed to have the form

$$\Delta f(x, Q^2) = N(\alpha_f, \beta_f, a_f)\, \eta_f\, x^{\alpha_f}(1-x)^{\beta_f}(1+a_f\, x), \quad (2)$$

where $N(\alpha, \beta, a)$ is fixed for each distribution by the normalization condition, $N(\alpha, \beta, a) \int_0^1 x^\alpha(1-x)^\beta(1+ax)\mathrm{d}x = 1$, and Δf denotes $\Delta\Sigma$, Δq^{NS}, or Δg. With this normalization the parameters η_g, η_{NS}, and η_Σ are the first moments of the polarized gluon distribution, the non-singlet quark distribution (in the proton or in the neutron), and the singlet quark distribution, respectively, at the initial scale. In this parametrization α_f and β_f determine the low-x and high-x behavior of the parton distribution, respectively. The polynomial describes the medium-x region and was included only for the parametrization of the singlet quark distribution. Some variations of the initial parton distributions were also tried in order to check the dependence of the results on the choice of the parametrization. The evolution was performed within the AB factorization scheme (in which $C_g^1 = -\frac{\alpha_s}{4\pi}$). The strong coupling constant $\alpha_s(M_Z^2)$ was taken to be 0.118 ± 0.003. The factorization scale M^2 and the renormalization scale μ^2 were taken to be $M^2 = k_1 \cdot Q^2$ and $\mu^2 = k_2 \cdot Q^2$, with $k_1 = k_2 = 1$. Further theoretical details of the fit procedure and analysis can be found in [15,19]. Following this scheme, the SMC performed a QCD analysis in NLO to existing polarized structure function data for proton, neutron and deuteron measured at SLAC, CERN and DESY [7,9,10, 12,11,13,14]. We repeated this fit and show the results for the best fit coefficients in Table 1. The world data on g_1^p are compared to the best fit in Fig. 2.

The first moment of the gluon distribution resulting from this fit is: $\eta_g = 0.9 \pm 0.3(\mathrm{exp}) \pm 1.0(\mathrm{theory})$ at $Q^2 =$

1 GeV^2. Similar results were obtained by an analysis performed by Altarelli et al. [19]. The experimental error depends on the statistical and systematic uncertainty in the measured data points, while the theoretical uncertainty comes mainly from the choice of the factorization and renormalization scales ($\delta\eta_g = \pm 0.6$), the initial parton distribution ($\delta\eta_g = \pm 0.5$) and the uncertainty in the value of α_s ($\delta\eta_g = \pm 0.3$). The polarized gluon distribution is deduced mostly from the observed scaling violations in the intermediate and low-x regions. Clearly the uncertainty on the size of the polarized gluon distribution is large. The existing data poorly constrain the low-x behavior of the various parton distributions and hence the values of α_Σ, α_g, and α_{NS}. Moreover different functional forms for the initial parton distributions result in different predictions for the low-x behavior of $g_1(x)$ as well as different values of the first moment of the polarized parton distribution [19], although the quality of the fit remains practically the same.

The behavior of g_1 at low x is still unknown. Unpolarized structure function data measured at HERA showed that F_2 rises at low x which is in agreement with pQCD [27], and for $Q^2 > 1$ GeV^2 does not follow a Regge behavior. For polarized DIS the low-x information is crucial to obtain a good determination of the moments of g_1 [10,18, 19]. In the past the extrapolation of g_1 from the measured region down to $x = 0$, required to obtain its first moment, was done assuming a Regge behavior of the structure function, which implies [28] $g_1 \propto x^{-\alpha}$ as $x \to 0$ with $0 \le \alpha \le 0.5$, i.e. a valence-like behavior of g_1. This behavior disagrees with that predicted by QCD. A comparison
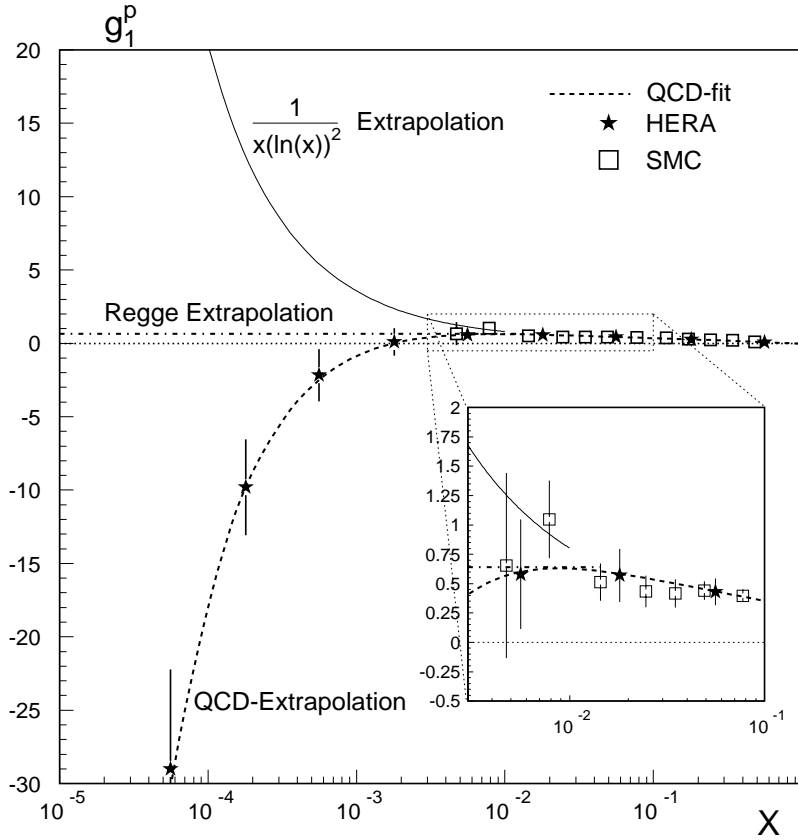
Fig. 3. The statistical uncertainty on the structure function g_1^p measurable at HERA for $Q^2 = 10$ GeV^2 with an integrated luminosity $\mathcal{L} = 500$ pb^{-1} and a comparison of various low-x behaviors of g_1^p. Also shown are the SMC measurements. Starting from the measured values of g_1^p by SMC, the possible values for g_1^p at low-x are shown for three scenarios: valence-like Regge behavior $g_1(x) \propto x^{-\alpha}$ with $\alpha = 0$, a strong powerlike positive rise $g_1(x) \propto 1/(x \cdot (\ln x)^2)$, and the pQCD prediction based on the present best fit. A detailed comparison in the low-x region of the SMC data is shown in the inset

between the Regge and QCD extrapolations from a recent analysis by the SMC [10] is shown in Fig. 3.

The low-x behavior has significant consequences on the first moment of g_1. While the integral in the measured x-range of $0.003 < x < 0.7$ amounts to $0.139 \pm 0.006(\text{stat.}) \pm 0.008(\text{syst.}) \pm 0.006(\text{evol.})$ at $Q^2 = 10$ GeV^2 (the last error is due to the uncertainty in the Q^2 evolution), the contribution from the unmeasured low-x range amounts to 0.002 or -0.011 depending on whether a Regge or a pQCD prescription is used to extrapolate into the low-x region. This provides the largest uncertainty on the first moment of g_1. Hence, an experimental measurement of the low-x behavior of g_1 would lead to significant insight on the validity of QCD.

3 Measurement of $g_1^p(x, Q^2)$ at HERA and its impact

Presently all measurements of polarized structure functions are made by deep inelastic lepton-nucleon scattering on fixed targets. To evaluate the impact of measurements in the extended kinematic range accessible at HERA, a detailed study has been performed assuming an integrated luminosity of $\mathcal{L} = 500$ pb^{-1}. After the planned luminosity upgrade of HERA [31] this would be achievable in about three years of data-taking. Beam polarizations were assumed to be 0.7 for electrons and protons. Kinematic cuts were applied based on standard analyses of data from the present detectors at the HERA collider [32,33]:

- the angle[1] of the scattered electron, θ'_e, is required to be $< 177^\circ$;
- the inelasticity y is limited to $0.01 < y < 0.9$;
- the energy of the scattered electron, E'_e, is required to be > 5 GeV;
- data were taken with $Q^2 > 1$ GeV^2.

A new parametrization [10] for the unpolarized structure function F_2, which includes recent data from NMC, E665, H1 and ZEUS was used. The SLAC parametrization [34] was used for the ratio R of longitudinal and transverse $\gamma^* p$ cross sections. Results for the expected number of events for different $x - Q^2$ bins are listed in Table 2, together with the average y, the depolarization factor $D = (y(2-y))/(y^2 + 2(1-y)(1+R))$, and the expected statistical uncertainty on the measured asymmetry δA_m. Standard deep inelastic scattering formulae [22,35] were used to calculate the kinematics and statistical uncertainties on the measured asymmetries. Using the best-fit parton distributions obtained from the QCD analysis of the data discussed in Sect. 2, predictions were made for $g_1(x, Q^2)$ values and hence for cross section asymmetries in the HERA range. Systematic uncertainties were not included and will be discussed at the end of this section. As shown in Fig. 1, measurements of g_1 at HERA will extend the x region down to $x = 5.6 \times 10^{-5}$. In Fig. 3 we show the expected accuracy of the determination of g_1 at HERA with the maximal extent of variation in the low-x behavior com-

---

[1]   Angles are defined with respect to the direction of the proton beam

Table 2. The kinematic variables x, Q^2, y, and D, with the number of events expected N_{total}, and the statistical uncertainty in the measured asymmetry δA_m assuming an integrated luminosity $\mathcal{L} = 500$ pb^{-1} and proton and electron beam polarizations $P_p = P_e = 0.7$

x	Q^2 GeV^2	y	D	N_{total}	δA_m
5.6×10^{-5}	1.8	0.40	0.47	3.8×10^6	5.1×10^{-4}
1.8×10^{-4}	1.8	0.13	0.13	6.9×10^6	3.8×10^{-4}
	5.6	0.40	0.46	2.8×10^6	6.0×10^{-4}
5.6×10^{-4}	1.8	0.04	0.04	1.0×10^7	3.1×10^{-4}
	5.6	0.13	0.13	4.9×10^6	4.5×10^{-4}
	1.8×10^1	0.40	0.47	1.4×10^6	8.6×10^{-4}
1.8×10^{-3}	1.8	0.01	0.01	1.4×10^7	2.7×10^{-4}
	5.6	0.04	0.04	7.3×10^6	3.7×10^{-4}
	1.8×10^1	0.13	0.13	2.4×10^6	6.4×10^{-4}
	5.6×10^1	0.40	0.47	6.9×10^5	1.2×10^{-3}
5.6×10^{-3}	5.6	0.01	0.01	9.2×10^6	3.3×10^{-4}
	1.8×10^1	0.04	0.04	3.6×10^6	5.3×10^{-4}
	5.6×10^1	0.13	0.13	1.2×10^6	9.3×10^{-4}
	1.8×10^2	0.40	0.47	3.1×10^5	1.8×10^{-3}
1.8×10^{-2}	1.8×10^1	0.01	0.01	4.1×10^6	4.9×10^{-4}
	5.6×10^1	0.04	0.04	1.5×10^6	8.3×10^{-4}
	1.8×10^2	0.12	0.13	5.1×10^5	1.4×10^{-3}
	5.6×10^2	0.40	0.47	1.3×10^5	2.8×10^{-3}
5.6×10^{-2}	5.6×10^1	0.01	0.01	1.4×10^6	8.5×10^{-4}
	1.8×10^2	0.04	0.04	4.4×10^5	1.5×10^{-3}
	5.6×10^2	0.12	0.13	1.4×10^5	2.7×10^{-3}
	1.8×10^3	0.40	0.47	3.7×10^4	5.2×10^{-3}
1.8×10^{-1}	1.8×10^2	0.01	0.01	3.1×10^5	1.8×10^{-3}
	5.6×10^2	0.04	0.04	9.8×10^4	3.2×10^{-3}
	1.8×10^3	0.13	0.13	2.8×10^4	6.0×10^{-3}
	5.6×10^3	0.40	0.47	6.9×10^3	1.2×10^{-2}
5.6×10^{-1}	5.6×10^2	0.01	0.01	1.4×10^4	8.4×10^{-3}
	1.8×10^3	0.04	0.04	3.9×10^3	1.6×10^{-2}
	5.6×10^3	0.13	0.13	9.8×10^2	3.2×10^{-2}
	1.8×10^4	0.40	0.47	2.1×10^2	6.9×10^{-2}

Fig. 4. Predicted values for g_1^p from NLO fits together with estimated statistical uncertainties for a future polarized DIS experiment with an integrated luminosity $\mathcal{L}=500$ pb^{-1} and with beam polarizations $P_e = P_p = 0.7$. The solid lines are predictions based on fits to present data extended into the HERA kinematic range, while the dotted and dashed lines are the predictions with a maximal and minimal gluon, respectively (see text)

patible with the requirement of integrability of g_1 (which implies that at small x g_1 can rise at most as $1/(x \ln^\alpha x)$ with $\alpha > 1$).

For the HERA measurements only one data point is shown at each x value, chosen to be the point with the smallest statistical errors which corresponds to the largest depolarization factor (see Table 2). The figure also shows that a polarized HERA can clearly distinguish between the different prescriptions for the g_1^p behaviors in the low-x region.

The measurable points with their estimated errors for HERA experiments are shown in Fig. 4 for eight accessible x-bins (out of the nine bins listed in Table 2). They are predicted on the basis of the NLO fit of Table 1, represented by the solid line. We also consider two limiting scenarios: a) the first moment of the gluon distributions is
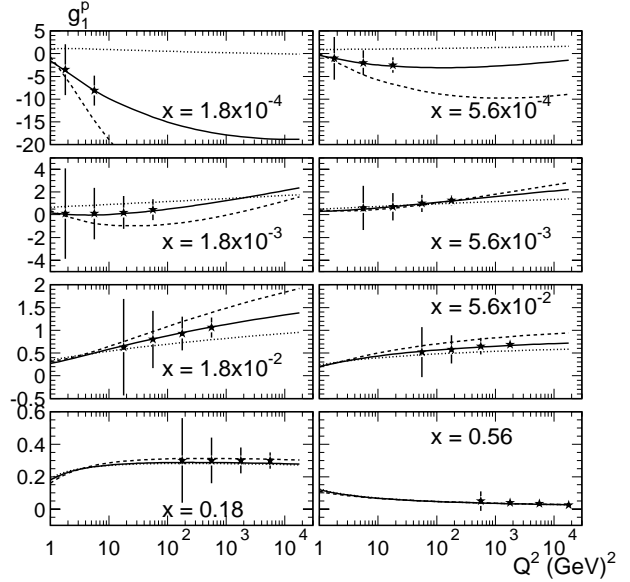
fixed to be 0 at $Q^2 = 1$ GeV^2 (minimal gluon: dashed lines in Fig. 4) and b) the first moment of the singlet quark density was fixed to $\eta_q = a_8$ at the same reference scale (maximal gluon: dotted lines in Fig. 4). Of course still wider deviations from these fits are possible since the low-x behavior of the current best fit is only very loosely constrained due to the lack of direct experimental information at low x. Furthermore, higher order corrections beyond NLO may turn out to be important at very low x [36,37].

The polarized gluon distribution is deduced from the scaling violations of g_1. Therefore a reasonably wide kinematic coverage is required in order to achieve such a determination with satisfactory accuracy. In particular, most of the present-day parametrizations of polarized parton distributions [15–17] indicate that $\Delta g(x, Q^2)$ is peaked in the unmeasured low-x region. Therefore data in this region with a large span in Q^2, such as those obtainable at HERA, would substantially improve the determination of $\Delta g(x, Q^2)$.

To assess the impact of these data we have repeated the QCD analysis described in Sect. 2 and included the projected HERA data. The values of g_1 at HERA predicted by the QCD analysis were randomized within their estimated statistical errors by assuming a Gaussian distribution. The values of the best-fit parameters (Table 1) of course remain the same within the errors, but the calculated statistical errors on the projected measurements, used in the QCD analysis provide an estimate on the reduction of the

experimental uncertainty in the fitted parameters. In Table 1 we compare the result of the fit with the projected HERA data to the analysis of present-day data only. Note in particular the sizable improvement in the determination of the first moment of Δg, from the present error $\delta(\eta_g) = \pm 0.3$ to ± 0.2 with HERA data. A similar improvement is observed for the uncertainty in α_g, which is determined by the low-x data. The theoretical uncertainty on the first moment of Δg as of today is large. The major contributing sources are factorization and renormalization scales, the initial parton distributions and the uncertainty in the value of α_s. At least the first two are direct consequences of the fact that g_1 structure function measurements are available from a rather small x and Q^2-range, namely $0.003 < x < 0.8$ and $1 < Q^2 < 100$ GeV^2. With HERA the measured x and Q^2-range would increase substantially, $10^{-5} < x < 0.8$ and $1 < Q^2 < 10^4$ GeV^2. Consequently the principal sources of theoretical uncertainty are expected to reduce significantly. Out of all the systematic uncertainties we tried to study the most dominant one, namely the factorization and renormalization scale uncertainty. This uncertainty is related to the lack of availability of higher than next-to-leading order corrections and is usually estimated by changing the scale factors, k_1, k_2 (see Sect. 2), in both directions (up and down), e.g. by a factor of two [19] or four [16]. The difference between the central value η_g^{best} and the one obtained from the fit which gives the largest deviation from η_g^{best} is assigned as the uncertainty on η_g due to the uncertainty in scales, $\delta_{scale}(\eta_g)$.

If we follow this procedure using the present day data, the $\delta_{\text{scale}}(\eta_g) \approx \pm 0.6$. In order to estimate the improvement one can expect in this uncertainty from future HERA data, this procedure was repeated with the projected data in Table 2. The QCD analysis fails to converge with the scale factors changed by factors of 4 or even 2, indicating that with HERA data, this uncertainty is constrained already. We repeated this procedure further by changing the scale factors by smaller amounts ($[k_1, k_2] = 0.5, 0.8, 1.2, 1.5$) with the requirement that the fit procedure should converge and result in fits with comparable χ^2-confidence level. The largest difference in value of η_g obtained from such a procedure compared to the one in our present best fit was $\delta_{\text{scale}}^{\text{HERA}} = \pm 0.15$. This suggests a possible improvement in this source of uncertainty by a factor of ≈ 4. This improvement is indicative of the reduction one could achieve in the total theoretical uncertainty in η_g from HERA data.

Systematic errors are discussed in [22,23]. The principal types of systematic errors associated with spin dependent asymmetry measurements are normalization errors and false asymmetries. The normalization errors are mainly due to uncertainties in the electron and proton beam polarizations P_e and P_p. These lead to a change in the magnitude of the measured asymmetry by an amount which is small compared to the statistical error, and hence they are important primarily when evaluating the first moment of $g_1^P(x)$.

Measurements of the electron polarization P_e at HERA by Compton scattering from polarized laser light have achieved [14,38] a relative uncertainty of 5%, and plans are being made to improve it to the 2% level which has already been achieved at SLAC [39]. Absolute measurement of the polarization of the high energy proton beam presents a new challenge and is presently under investigation at RHIC and at HERA. It is reasonable to expect that an accuracy of 5% can be achieved [40–43]. The polarization errors of 2% (5%) translate directly into a relative error of 2% (5%) on the structure function g_1.

The other type of systematic error, which is due to false asymmetries, arises from time variations in detector efficiencies between the measurements for the parallel and antiparallel spin conditions, and the correlation of proton polarization with the beam intensity or the bunch crossing angle. With regard to the time variation of detector efficiencies, the interaction region for proton and electron bunches should be the same for different proton spin orientations, thus keeping the detector acceptance constant. In the polarized HERA collider we expect to run in a mode where a sequence of about 10 proton bunches will have a given polarization, and the next sequence will have the opposite polarization. Since the time interval between the successive bunch crossings is 96 ns, the asymmetry measurements will be done within 2 μs and for such a time scale the detector efficiencies should be constant. A possible correlation between proton bunch intensity and polarization can lead to a false asymmetry, which can be avoided by repeating the measurements after rotation of all the proton spins. Small contributions to false asymmetries may arise due to the correlations with the proton spin direction of the micro-structure and polarization distribution within a bunch which can also be eliminated by the proton spin rotation. A further possible source of false asymmetries comes from potential asymmetries of background contamination in the ep sample, namely interactions of the beams with beam-gas. Present analyses at HERA have achieved data samples with a purity of better than 99%. Furthermore, residual asymmetries caused by such background interactions can be efficiently monitored by using so-called pilot bunches, i.e. bunches which pass the interaction region and have no collision partner in the other beam. Therefore this source of systematics can be kept smaller than 10^{-4}. Hence we believe that false asymmetries at polarized HERA can be controlled at the required level of 10^{-4} or less. Similar requirements are necessary for the RHIC-SPIN program and are being actively studied. More quantitative estimates can not be made at this time, since they depend on the polarized collider parameters and operating conditions which are being studied at DESY.

We conclude that introduction of systematic errors will not change significantly our conclusions on the impact of future HERA g_1 data. This conclusion also applies to radiative corrections, which have been studied for the HERA kinematics in [44] and we checked, using the program HECTOR 1.11 [45], that they are well under control.
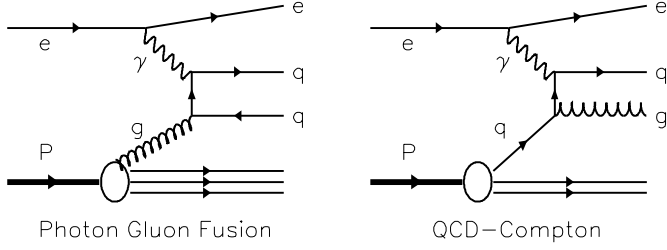
Fig. 5. Feynman diagrams for the processes contributing to the di-jet cross section at LO: the Photon-Gluon Fusion (PGF) process (left) and the QCD-Compton (QCDC) process (right)

4 A direct measurement of $\Delta g(x, Q^2)$ from di-jet events at HERA

From the discussion in Sect. 3 it appears that the polarized gluon distribution $\Delta g(x, Q^2)$ is not as well constrained by the Q^2 dependence of the structure function as is the un-polarized gluon density. In fact, while the first moment of the polarized gluon density can be deduced from scaling violations (including future HERA data) within 20%, the shape of $\Delta g(x)$ is not constrained. Therefore measurements which are directly sensitive to $\Delta g(x, Q^2)$ are of great interest and are expected to add important information to the determination of not only the first moment of Δg but also of its shape. It has been shown by H1 at HERA [5] that in leading order (LO) the unpolarized gluon momentum distribution, $g(x)$, can be accessed in a direct way by measuring the cross section of di-jet production in DIS in a region of $Q^2 = 5 - 50$ GeV^2 with both jets measured in the central detector (the proton remnant jet is not counted), and for jets with a transverse energy E_T larger than 5 GeV. In leading order two processes contribute to the di-jet events, Photon-Gluon Fusion (PGF) and QCD-Compton scattering (QCDC), both leading to two jets back to back in azimuth in the hadronic center-of-mass system. The Feynman diagrams for the two processes are shown in Fig. 5. The PGF cross section is proportional to $\alpha_s g(x)$. The QCDC cross section, however, is proportional to $\alpha_s q(x)$ and constitutes the background. The kinematic parameters to describe the PGF process are the momentum fraction of the proton carried by the gluon x_g, the four-momentum transfer Q^2 and the invariant mass of the two jets $\hat{s}$. They are related to the Bjorken-x, by:

$$x_g = x(1 + \frac{\hat{s}}{Q^2}).$$

For $\hat{s} > 100$ GeV^2, x_g is larger than x by about an order of magnitude and the accessible range at HERA is about $0.002 < x_g < 0.2$.

The feasibility of using this kind of measurement in the case of polarized lepton-nucleon scattering to extract $\Delta g(x, Q^2)$ from di-jet asymmetries has been discussed in [47,48]. A new study of such a measurement at HERA has been performed and is detailed in [49]. Recently NLO corrections were calculated for the polarized jet rates and found to be small [50]. In this paper we summarize the

main results and use the projected data to assess the sensitivity to the shape of $\Delta g(x, Q^2)$. In LO the total unpolarized di-jet cross section is the sum of the contributions from PGF processes and QCDC scattering, and can be written as:

$$\sigma_{\mathrm{di-jet}} = \sigma_{\mathrm{di-jet}}^{\mathrm{PGF}} + \sigma_{\mathrm{di-jet}}^{\mathrm{QCDC}} = A \, g + B \, q \qquad (3)$$

where g and q are the gluon and quark densities. A and B can be calculated in perturbative QCD. Similarly, for the polarized case we can write:

$$\Delta\sigma_{\mathrm{di-jet}} = \sigma_{\mathrm{di-jet}}^{\uparrow\downarrow} - \sigma_{\mathrm{di-jet}}^{\uparrow\uparrow} = a \, \Delta g + b \, \Delta q \qquad (4)$$

with Δg and Δq being the polarized gluon and quark densities. The left arrow in the subscript denotes the polarization of the incoming lepton with respect to the direction of its momentum. The right arrow stands for the polarization of the proton being anti-parallel or parallel to the polarization of the incoming lepton. The di-jet asymmetry is sensitive to $\Delta g/g$, especially at low x where the PGF cross section dominates.

$$A_{\mathrm{di-jet}} = \frac{\Delta\sigma_{\mathrm{di-jet}}}{2\,\sigma_{\mathrm{di-jet}}} \qquad (5)$$

$$= \mathcal{A} \, \frac{\Delta g}{g} \, \frac{\sigma_{\mathrm{di-jet}}^{\mathrm{PGF}}}{2\,\sigma_{\mathrm{di-jet}}} + \mathcal{B} \, \frac{\Delta q}{q} \, \frac{1}{2} \, (1 - \frac{\sigma_{\mathrm{di-jet}}^{\mathrm{PGF}}}{\sigma_{\mathrm{di-jet}}}),$$

with $\mathcal{A} \equiv a/A$ and $\mathcal{B} \equiv b/B$. The experimentally accessible asymmetry A_{meas} is related to $A_{\mathrm{di-jet}}$ by

$$A_{\mathrm{meas}} = \frac{N^{\uparrow\downarrow} - N^{\uparrow\uparrow}}{N^{\uparrow\downarrow} + N^{\uparrow\uparrow}} = P_e P_p D A_{\mathrm{di-jet}} \qquad (6)$$

where D is the depolarization factor and A_{meas} is the measured asymmetry. The quantities $N^{\uparrow\downarrow}$ ($N^{\uparrow\uparrow}$) are the total number of observed di-jet events ($N^{\uparrow\downarrow} = N_{\mathrm{PGF}}^{\uparrow\downarrow} + N_{\mathrm{QCDC}}^{\uparrow\downarrow}$) for antiparallel (parallel) proton and electron spins.

A Monte Carlo study was performed for a polarized HERA on the expected size and uncertainty of the measured di-jet asymmetries and the contributions from signal and background processes. PEPSI 6.5 [51] was used, which is a full LO lepton-nucleon scattering Monte Carlo program for unpolarized and polarized interactions, including fragmentation, and unpolarized parton showers to simulate higher order effects. On the parton level the results were cross checked using the Monte Carlo cross section integration program [52]. Detector smearing and acceptance effects were included based on the performance of the present H1 detector. As input for the unpolarized parton distributions we used the LO GRV parametrizations [53] and for the polarized distributions various published parametrizations, as well as the result for Δg of the NLO fit described in the previous section were used. All these distributions are in agreement with the present data. Monte Carlo events were generated for an integrated luminosity of 500 pb^{-1} and beam polarizations of 0.7 for electron and proton beams. Jets were defined by the cone jet algorithm with a cone radius of 1 in the pseudorapidity η and azimuthal angle ϕ plane. Di-jet events were selected by the following criteria:

Table 3. a Expected measured asymmetries from di-jet events for six x_g-bins with a polarized HERA and background corrected asymmetries with statistical errors corresponding to an integrated luminosity of 500 pb^{-1}, **b** The background corrected asymmetries for two different Q^2 ranges

a)	$5 < Q^2 < 100$ GeV^2		
x_g	A_{meas}	A_{corr}	$\delta(A)$
0.002	-0.003	-0.003	0.005
0.006	-0.008	-0.008	0.003
0.014	-0.013	-0.013	0.004
0.034	-0.030	-0.030	0.006
0.084	-0.031	-0.042	0.012
0.207	-0.023	-0.047	0.027

b)	$2 < Q^2 < 10$ GeV^2		$10 < Q^2 < 100$ GeV^2	
x_g	A_{corr}	$\delta(A)$	A_{corr}	$\delta(A)$
0.002	-0.006	0.005	-0.001	0.007
0.006	-0.010	0.003	-0.006	0.003
0.014	-0.011	0.004	-0.015	0.004
0.034	-0.033	0.007	-0.029	0.007
0.084	-0.041	0.013	-0.035	0.013
0.207	-0.091	0.027	-0.013	0.031

– two jets with $E_T > 5$ GeV;
– 5 GeV$^2 < Q^2 < 100$ GeV^2;
– $0.3 < y < 0.85$;
– $\hat{s} > 400\,(100)$ GeV^2.

The invariant mass of the two jets is reconstructed from their four-momenta $P_{1(2)}$: $\hat{s} = (P_1 + P_2)^2$. The cut $\hat{s} > 400$ GeV^2 was chosen to keep higher order corrections small [50]. However, the data with $100 < \hat{s} < 400$ GeV^2 were also analyzed. The asymmetries were found to be as large as a few percent and are listed in Table 3a.

The two lowest x_g-bins in the table are obtained from the lower $\hat{s}$ data. In this table the asymmetry corrected for QCDC background ($A_{\mathrm{corr}} = A_{\mathrm{meas}} - \frac{N_{\mathrm{QCDC}}^{\uparrow\downarrow} - N_{\mathrm{QCDC}}^{\uparrow\uparrow}}{N^{\uparrow\downarrow} + N^{\uparrow\uparrow}}$) is also presented. Note that there is a significant QCDC contribution only for the two highest x_g-bins.

Figure 6 shows the projected values of $\Delta g(x)/g(x)$ and $x\Delta g(x)$ as a function of x_g for $\mathcal{L} = 500$ pb^{-1} for different $\Delta g(x, Q^2)$ distributions: the polarized gluon density obtained from the NLO fit to g_1 data by the SMC, the gluon set C by Gehrmann and Stirling [17] and an instanton-induced gluon proposed by Kochelev [54]. The results are presented at $Q^2 = 20$ GeV^2 which is very close to the average Q^2 of the simulated data.

The shaded error band shows an estimate of the systematic uncertainty considering the following error sources: an uncertainty of 2% on the calibration of the hadronic energy scale, the error on the total unpolarized di-jet cross section of 2% and on the unpolarized gluon density $g(x)$ of 5% [55]. The uncertainty on the ratio of the polarized and unpolarized quark densities, $\Delta q/q$, was considered to be 10% and the error on the polarization measurements for electron and proton beams was taken to be 5%. Both statistical and systematic errors were calculated [49] using as

input the gluon set A of Gehrmann and Stirling [17], which resembles the gluon distribution extracted from the NLO fit to g_1, and were adjusted to the different parametrizations used here.

It can be seen that the measurement is sensitive to the different gluon distributions, and that its shape can be determined with six bins in x. Using these projected measurements the statistical error of the first moment of Δg in the x-range of 0.0015–0.32 is: $\delta(\int_{0.0015}^{0.32} \Delta g(x)\mathrm{d}x) = 0.2$.

A further study was performed using additional information on the Q^2 dependence. For this study we extended the Q^2 range down to 2 GeV^2 and divided the data into two bins with: $2 < Q^2 < 10$ GeV^2 and $10 < Q^2 < 100$ GeV^2. The expected sensitivity on $\Delta g(x, Q^2)$, reflected by the expected asymmetries and their errors, is shown in Table 3b. The mean Q^2 values for the two bins are 4.5 and 30 GeV^2, respectively. The effect of the Q^2 evolution of the gluon can be seen, but does not appear to be very large.

5 Combined QCD analysis of g_1 data and Δg from di-jet asymmetries

The measurement of $g_1(x, Q^2)$ and di-jet asymmetries provide complementary information on the polarized gluon distribution. As argued in Sects. 3 and 4 the first moment of the polarized gluon distribution can be obtained from the QCD analysis in NLO of g_1 data while di-jet asymmetries will provide a direct measurement of the polarized gluon density $\Delta g(x, Q^2)$ in the range $0.0015 < x < 0.32$. Hence, it is interesting to study the impact of a combined analysis of g_1 and di-jet asymmetry data on the determination of Δg.

In principle, such an analysis should be carried out using the measured di-jet asymmetries and g_1 data in a self-consistent procedure in NLO. Polarized quark and gluon densities should be fitted simultaneously to both data sets, in order to reproduce the scaling violations in g_1 and separate the PGF and QCDC contributions to the jet asymmetry cross sections. The tools to perform such analysis are not available yet. However, the effect of the combined analysis on the uncertainty in Δg can be assessed by including the values of $\Delta g(x, Q^2)$ obtained from the di-jet analysis in the NLO QCD fit of the g_1 data as an extra constraint.

The values of $\Delta g(x, Q^2)$ in the six x-bins, as obtained from the analysis of di-jet asymmetries, were considered as data. Statistical errors were obtained from the Monte Carlo simulation discussed in Sect. 4. The values used for $\Delta g(x, Q^2)$ were taken from the best fit of present-day g_1 data described in Sect. 2. Like the projected g_1 data for the HERA kinematic region, they were randomized around the calculated value within one standard deviation of the statistical error. As mentioned in Sect. 3, including the projected g_1 data in the NLO analysis, reduced the error on the first moment of Δg by about 30%, yielding $\eta_g = 0.9 \pm 0.2$, down from $\delta(\eta_g) = 0.3$. The QCD analysis of the present and the projected g_1 data was repeated
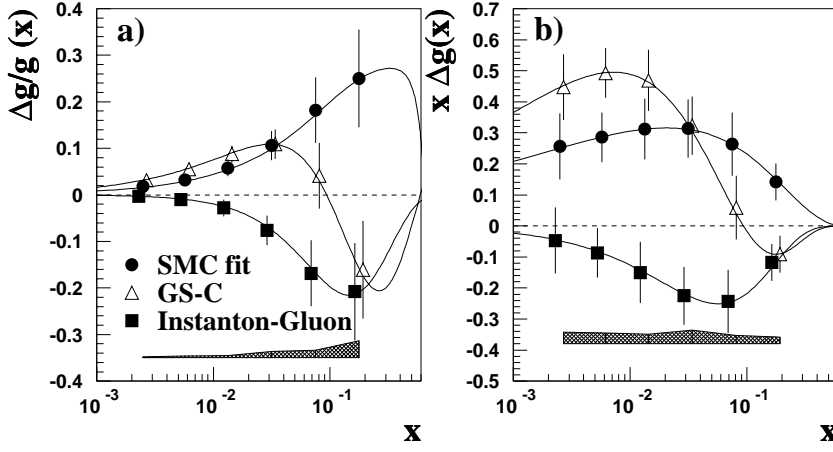
Fig. 6. a The sensitivity to $\Delta g(x)/g(x)$, and b $x\Delta g(x)$ from a measurement of di-jet events with a polarized HERA at $Q^2 = 20$ GeV^2 assuming an integrated luminosity of 500 pb^{-1}. The error bars show the expected statistical error. An estimate of systematic uncertainties is reflected in the shaded error band. As input for the parton distributions three different parametrizations were used (see text)
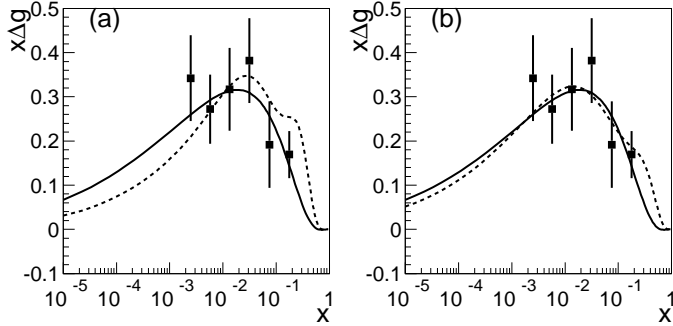

Fig. 7. a The polarized gluon distribution at $Q^2 = 20$ GeV^2 obtained from a 14 parameter fit (3), dashed line, including only existing g_1 data, b including existing and projected g_1 and $\Delta g(x)$ data. For comparison also the results of the 10 parameter fit to existing and projected data is shown, solid line, as well as the corresponding Δg values with their statistical errors, as they could be obtained from a di-jet analysis

Table 4. The expected uncertainty in the determination of the first moment of the gluon distribution at $Q^2 = 1$ GeV^2 with inclusive and di-jet data from polarized HERA with $\mathcal{L} = 500$ pb^{-1}

Data used	$\delta(\int \Delta g)$
QCD Anal. of published g_1 today (= "A")	± 0.3
"A" + Projected HERA g_1^{P}	± 0.2
"A" + Projected HERA Δg-jets	± 0.2
"A" + Projected HERA g_1^{P} and Δg-jets	± 0.1

$$N(\alpha_f, \beta_f, a_f)\ \eta_f\ x^{\alpha_f}(1-x)^{\beta_f}(1 + a_f\ x + b_f\ \sqrt{x}).$$

Using this form in the QCD analysis of the g_1 data results in a fit with a node in $\Delta g(x,Q^2)$, which is not allowed by the more restricted form of (2). The gluon distribution obtained from a fit with this functional form is shown in Fig. 7 where it is also compared with the gluon distribution obtained with the standard form (2). While the first moment of Δg at $Q^2 = 1$ GeV^2 is 0.9 ± 0.3, the same value as obtained in the standard fit, the shapes of the gluon distributions are different.

On the other hand, di-jet asymmetries provide good information on the shape of the polarized gluon distribution in the measured region. The effect of the additional data on our knowledge of Δg can be demonstrated when the projected values of g_1 and $\Delta g(x,Q^2)$, (obtained from the standard, 10 parameter fit) are fitted with 14 parameters, as discussed above. As shown in Fig. 7, once all the projected g_1 and di-jet data are included in the fit, the polarized gluon distribution obtained from the 14 parameter fit is essentially identical to that obtained from the 10 parameter fit in the region where $\Delta g(x,Q^2)$ data are introduced. Obviously, $\Delta g(x,Q^2)$ remains unconstrained in the high x region where no $\Delta g(x,Q^2)$ data is added and where the Q^2 evolution is small. One may thus conclude that the combined analysis will constrain the functional form of the polarized gluon distribution in addition to its first moment.

including also $\Delta g(x,Q^2)$ values from the di-jet asymmetries in the fit. While the best fit parameters are obviously about the same as those obtained for the NLO fit of the g_1 data, the uncertainty on the first moment of the polarized gluon distribution is reduced by 50%, resulting in $\eta_g = 1.0 \pm 0.1$. The polarized gluon distribution from the best fit of g_1 data, and projected HERA data, evolved to 20 GeV^2 is shown in Fig. 7 along with the projected data of $\Delta g(x,Q^2)$ used in the fit. The effect of the di-jet data alone on the uncertainty in η_g is similar to that of the additional g_1 data which will be measured at HERA. The combined fit of present-day g_1 data with the $\Delta g(x,Q^2)$ from di-jet asymmetries yields $\eta_g = 1.0 \pm 0.2$. The results for the first moments of the polarized gluon distributions obtained from the fit of g_1 data with projected g_1 and Δg data are summarized in Table 4.

While the first moment of the polarized gluon distribution can be deduced from scaling violations in g_1, the QCD analysis does not constrain its shape. This can be demonstrated by introducing an additional term, $b_f\sqrt{x}$ into the functional form of the parton distributions,

$$\Delta f(x,Q^2) = \qquad\qquad (7)$$

6 Conclusions

Inclusive polarized DIS measurements at HERA with polarized protons and with a high integrated luminosity will yield significant and unique new information on $g_1^{\mathrm{p}}(x, Q^2)$ over a much extended range in x and Q^2, which is of great theoretical interest. Statistical errors on the points will dominate. For such measurements the false asymmetries should be considerably smaller than the true asymmetries to be measured, and normalization errors should be controlled to be better than 10%.

The present uncertainties in the determination of the first moment of the polarized gluon distribution are large. They will be considerably reduced by the pQCD analysis of the g_1 structure function data from HERA. However we have shown that even further reduction in the uncertainty can be achieved if polarized gluon information coming from the di-jet events is used in the analysis in conjunction with the g_1 data.

The fact that HERA is an operating facility with a plan for substantial increase in luminosity and with two major operating detectors, as well as a polarized electron beam, means that only the high energy polarized proton beam needs to be developed. The efforts to achieve this goal seem well justified and data from such experiments at HERA would provide unique and complementary information to that from other presently proposed experiments.

References

1. R. Hofstadter, Rev. Mod. Phys. **28** (1956) 214
2. J. Friedman et al., Ann. Rev. Nucl. Science **22**, (1972), 203
3. EMC, J. Aubert et al., Phys. Lett. **B123** (1982) 275; NMC, M. Arneodo et al., Phys. Lett. **364** (1995) 107; BCDMS Collaboration, A.C. Benvenuti et al., Phys. Lett. **B223** (1989) 490
4. ZEUS Collaboration, M. Derrick et al., Phys. Lett. **B316** (1993) 412; H1 Collaboration, I. Abt et al., Nucl. Phys. **B407** (1993) 515
5. H1 Collaboration, S. Aid et al., Nucl. Phys. **B445** (1995) 3
6. SLAC E80, M.J. Alguard et al., Phys. Rev. Lett. **37** (1976) 1261; ibid **41** (1978) 70; SLAC E130, G. Baum et al., Phys. Rev. Lett. **51** (1983) 1135; V.W. Hughes and J. Kuti, Ann. Rev. Nucl. Part. Sci. **33**, (1983) 611
7. EMC, J. Ashman et al., Phys. Lett. **B206** (1988) 364; Nucl. Phys. **B328** (1989) 1
8. G. Altarelli and G. Ridolfi, Nucl. Phys. B Proc. Suppl. **39B** (1995) 106
9. SMC, B. Adeva et al., Phys. Lett. **B302** (1993) 533; SMC, D. Adams et al., Phys. Lett. **B329** (1994) 399; SMC, D. Adams et al., Phys. Lett. **B357** (1995) 248; SMC, D. Adams et al., Phys. Lett. **B396** (1997) 338; SMC, D. Adams et al., Phys. Rev. **D56** (1997) 5330
10. SMC, B. Adeva et al., Phys. Lett. **B412** (1997) 414
11. E143 Collaboration, K. Abe et al., Phys. Rev. Lett. **74** (1995) 346; E143 Collaboration, K. Abe et al., Phys. Rev. Lett. **75** (1995) 25; E143 Collaboration, K. Abe et al., Phys. Lett. **B364** (1995) 61
12. E142 Collaboration, P.L. Anthony et al., Phys. Rev. Lett. **71** (1993) 959; E142 Collaboration, P.L. Anthony et al., Phys. Rev. **D54** (1996) 6620
13. E154 Collaboration, K. Abe et al., Phys. Rev. Lett. **79** (1997) 26
14. HERMES Collaboration, K. Ackerstaff et al., Phys. Lett. **B404** (1997) 383
15. R.D. Ball, S. Forte and G. Ridolfi, Phys. Lett. **B378** (1996) 255
16. M. Glück et al., Phys. Rev. **D53** (1996) 4775
17. T. Gehrmann and W.J. Stirling, Z. Phys. **C65** (1995) 461; Phys. Rev. **D53** (1996) 6100
18. E154 Collaboration, K. Abe et al., Phys. Lett. **B405** (1997) 180
19. G. Altarelli et al., Nucl. Phys. **B496** (1997) 337
20. D.P. Barber, Polarized Protons in HERA, Proceedings of the 2nd SPIN workshop "Theory meets experiment", ed.s J. Blümlein and W.-D. Nowak, Zeuthen (1997); "Acceleration of Polarized Protons to 820 GeV at HERA", SPIN collaboration and DESY Polarization Team, Nov. 8, 1996
21. J. Blümlein, Proceedings of the "Workshop on the Prospect of Spin Physics at HERA", ed.s J. Blümlein and W.-D. Nowak, DESY-Zeuthen, DESY-95-200 (1995) 179; V.W. Hughes et al., ibid., 350
22. R.D. Ball et al., hep-ph/9609515 and in Proceedings of workshop "Future Physics at HERA", ed.s G. Ingelman, A. De Roeck and R. Klanner, DESY (1996) 777
23. A. Deshpande, V.W. Hughes and J. Lichtenstadt, Proceedings of workshop "Future physics at HERA with polarized protons", ed.s A. De Roeck and T. Gehrmann, DESY (1997)
24. V.N. Gribov and L.N. Lipatov, Sov. Journ. Nucl. Phys. **15** (1972) 438 and 675; G. Altarelli and G. Parisi, Nucl. Phys. **B126** (1977) 298; Yu. L. Dokshitzer, Sov. Phys. JETP **46** (1977) 641
25. J. Kodaira et al., Phys. Rev. **D20** (1979) 627; J. Kodaira, Nucl. Phys. **B165** (1980) 129
26. R. Mertig and W.L. van Neerven, Z. Phys. **C70** (1996) 637; W. Vogelsang, Nucl. Phys. **B475** (1996) 47
27. R.D. Ball and A. De Roeck, hep-ph/9609309 and Proceedings of workshop "DIS96", ed.s G. D'Agostini and A. Nigro, World Scientific, Singapore (1996), 669
28. R.L. Heimann, Nucl. Phys. **B64** (1973) 429
29. Particle Data Group, R.M. Barnett et al., Phys. Rev. **D54** (1996) 1
30. F.E. Close and R.G. Roberts, Phys. Lett. **B316** (1993) 165
31. W. Bartel at al., Proceedings of workshop "Future Physics at HERA", ed.s G. Ingelman, A. De Roeck and R. Klanner, DESY (1996) 1093
32. H1 Collaboration, S. Aid et al., Nucl. Phys. **B470** (1996) 3
33. ZEUS Collaboration, M. Derrick et al., Z. Phys. **C72** (1996) 399
34. L.W. Whitlow et al., Phys. Lett. **B250** (1990) 193 and L.W. Whitlow, PhD thesis, Stanford University, 1990
35. T. Pussieux and R. Windmolders, in "Internal Spin Structure of the Nucleon", ed.s V. W. Hughes and C. Cavata, World Scientific, Singapore (1995); also DAPNIA-SPHN-95-10 preprint

36. J. Blümlein and A. Vogt, Phys. Lett. **B370** (1996) 149; ibid. **B386** (1996) 350
37. J. Bartels, B. Ermolaev and M. Ryskin, Z. Phys. **C70** (1996) 273; ibid. **C72** (1996) 627
38. D.P. Barber et al., Nucl. Instr. and Meth. **A329** (1993) 79
39. SLD Collaboration, K. Abe et al., Phys. Rev. Lett. **78** (1997) 2075
40. P. Schüler: Summary of Workshop on High Energy Collider Spin Physics at RHIC and HERA , BNL, August 25,26 1997; Presentations by Z. Meziani, T. Chupp and M. Ramolis
41. E. Leader, Review of the theoretical workshop on proton beam polarimetry, BNL, Proceedings of the 2nd SPIN workshop "Theory meets experiment", ed.s J. Blümlein and W.-D. Nowak; Zeuthen (1997)
42. "Acceleration of Polarized Protons to 120 GeV and 1 TeV at Fermilab", Michigan preprint HE 95-09, (1995)
43. M. Beddo et al., Proposal for spin physics at RHIC (1993)
44. D. Bardin et al., hep-ph/9711228 and Proceedings of the 2nd SPIN workshop "Theory meets experiment", ed.s J. Blümlein and W.-D. Nowak; Zeuthen (1997)
45. A. Arbuzov et al., Comp. Phys. Commun. **94** (1996) 128, hep-ph/9511434; D. Bardin et al., Nucl. Phys. **B506** (1997) 295
46. E. Mirkes and C. Ziegler, Nucl. Phys. **B429** (1994) 93
47. J. Feltesse, F. Kunne and E. Mirkes, Phys. Lett. **B388** (1996) 832
48. A. De Roeck et al., hep-ph/9610315 and Proccedings of workshop "Future physics at HERA", ed.s G. Ingelman, A. De Roeck, R. Klanner, DESY (1996) 803
49. G. Rädel, A. De Roeck and M. Maul, hep-ph/9711373 and Proccedings of workshop "Future physics at HERA with polarized protons", ed.s A. De Roeck and T. Gehrmann, DESY (1997)
50. E. Mirkes and S. Willfahrt, hep-ph/9711434 and Proceedings of workshop "Future physics at HERA with polarized protons", ed.s A. De Roeck and T. Gehrmann, DESY (1997)
51. L. Mankiewicz, A. Schäfer and M. Veltri, Comp. Phys. Comm. **71** (1992) 305; M. Maul et al., hep-ph/9710434
52. E. Mirkes, D. Zeppenfeld , Phys. Lett. **B380** (1996) 205
53. M. Glück, E. Reya and A. Vogt, Z. Phys. **C67** (1995) 433
54. N.I. Kochelev et al. ,hep-ph/9711226 and Proceedings of the 2nd SPIN workshop "Theory meets experiment",ed.s J. Blümlein and W.-D. Nowak, Zeuthen (1997). Proceedings of workshop "Future physics at HERA with polarized protons", ed.s A. De Roeck and T. Gehrmann, DESY (1997)
55. M. Botje, M. Klein and C. Pascaud, Proceedings of workshop "Future physics at HERA", ed.s G. Ingelman, A. De Roeck, R. Klanner, DESY (1996) 33